Quantifying vapor transfer into evaporating ethanol drops in humid atmosphere

Journal:	*Physical Chemistry Chemical Physics*
Manuscript ID	CP-ART-04-2018-002521.R2
Article Type:	Paper
Date Submitted by the Author:	27-Jun-2018

Complete List of Authors:	Kita, Yutaku; I2CNER, Kyushu University, Thermal Science and Engineering Research Division; Kyushu University, Mechanical Engineering Okauchi, Yuya; Kyushu University, Mechanical Engineering Fukatani, Yuki; Toshiba Corporation Research and Development Center Orejon, Daniel; I2CNER, Kyushu University, Thermal Science and Engineering Research Division; Kyushu University, Mechanical Engineering Kohno, Masamichi ; Kyushu University Takata, Yasuyuki; International Institute for Carbon-Neutral Energy Research; I2CNER, Kyushu University, Thermal Science and Engineering Research Division; JST-CREST, Japan Society and Technology Agency Sefiane, Khellil; University of Edinburgh, School of Engineering

Quantifying vapor transfer into evaporating ethanol drops in humid atmosphere

Yutaku Kita[1,2], Yuya Okauchi[2], Yuki Fukatani[3], Daniel Orejon[1,2*], Masamichi Kohno[2], Yasuyuki Takata[1,2,4], Khellil Sefiane[5]

[1]International Institute for Carbon-Neutral Energy Research (WPI-I[2]CNER), Kyushu University, 744 Motooka, Nishi-ku, Fukuoka 819-0395, Japan
[2]Department of Mechanical Engineering, Thermofluid Physics Laboratory, Kyushu University, 744 Motooka, Nishi-ku, Fukuoka 819-0395, Japan
[3]Toshiba Corporation, Kanagawa 230-0045, Japan
[4]JST-CREST, Japan Science and Technology Agency, 744 Motooka, Nishi-ku, Fukuoka 819-0395, Japan
[5]Institue of Multiscale Thermofluids, School of Engineering, The University of Edinburgh, King's Buildings, Mayfield Road, Edinburgh EH9 3JL, United Kingdom

*corresponding author: orejon.daniel@heat.mech.kyushu-u.ac.jp

Abstract

The effect of ambient temperature and relative humidity on the dynamics of ethanol drop evaporation is investigated. Although drop evaporation of mixtures and pure fluids has been extensively studied, very little is known about the transition from pure fluid to a binary mixture following transfer of a second component present in the atmosphere. This is of importance for industrial, biological and medical applications where the purity of the solvent is paramount. Adsorption-absorption and/or condensation of water into ethanol drops during evaporation is presented through direct quantification of the drop composition in time. In particular, we combine drop profile measurements with Gas Injection Chromatography (GIC) to directly quantify the amount of ethanol evaporated and that of water intake over time. As expected, drops evaporate faster at higher temperatures since both ethanol saturation concentration and vapor diffusion coefficient are directly proportional to temperature. On the other hand, the increase in the ethanol evaporation rate and in the water intake are observed at higher relative humidity. The increase in ethanol evaporation at higher relative humidity is interpreted by the increase in diffusion coefficient of ethanol into humid air when compared to dry air. Moreover, as ethanol evaporates in a high humidity environment, the drop interfacial temperature falls below the dew point due to evaporative cooling and water condenses compared to lower humidity conditions. As a consequence of the heat released by adsorption-absorption and/or condensation, greater temperature is reported at the liquid-vapor interface as confirmed by IR thermography, inducing greater ethanol saturation concentration at the surface and hence greater driving force for evaporation. By coupling drop profile and composition of ethanol and water within the drop, we propose a combined evaporation-absorption/adsorption and/or condensation empirical correlation. The proposed correlation accounts for: the decreases in ethanol concentration due to water absorption-adsorption and/or condensation, for the diffusion coefficient dependence on relative humidity, and for the amount of water intake during evaporation. The proposed empirical correlation agrees remarkably well with experimental observations.

Introduction

Substrate wettability, roughness, conductivity, temperature, and/or fluid properties are well known factors influencing the complex phenomena of wetting and evaporation of liquids on solid surfaces[1-9]. In addition to these factors, the effect of the surrounding atmosphere also has a strong effect on drop evaporation[10-14]. Houghton first and then Fuchs few decades later, reported the first experimental observations on the effect of relative humidity and surrounding atmosphere on water drop evaporation[10, 11]. Accordingly to Fick's first law, the lifetime of a suspended spherical drop is function of the concentration of its vapor in the atmosphere[12, 14]. In other words, a water drop eventually evaporates faster in atmospheres with low relative humidity. This is consistent with the increase in the evaporation rate of water drops evaporating in inert atmospheres[13, 15]. Furthermore the effect of relative humidity[16, 17], presence of volatile organic compounds[18, 19], reduced pressure[15, 20-22], presence of particles as suspension[23-25], dissolved salts,[26] polymers,[27] and/or the application of external forces[28-30] on the evaporative behavior of volatile liquid drops have also been recent subjects of study.

In addition to the aforementioned investigations on pure liquid drops, wetting and evaporation of binary mixtures have also received important attention in the past decades[31-35]. Evaporation of binary mixtures are relevant to many industrial and biomedical applications such as material processing[36], patterning[37], DNA chip manufacturing[38] and thermal management[39], amongst others. Propanol-water[34], ethanol-water[40-43] and methanol-water[44] are some of the binary mixtures reported to exhibit distinctive wetting and evaporation behaviors when compared to pure fluids. Looking at the evolution of contact angle and contact radius during evaporation of ethanol-water mixtures on a PTFE substrate, Sefiane *et al.* reported three stages of evaporation [40]. Thereafter, Particle Image Velocimetry (PIV) revealed that the first stage of evaporation is characterized by random orientation and unsteady radial velocities within the drop, which are driven by concentration and temperature gradients[41]. This is followed by a transition

stage and eventually, after ethanol completely evaporates, the drop vanishes following the same behavior as that of pure water. Other recent approaches used for flow visualization within evaporating drops are spectral radar optical coherence tomography[45], high speed confocal microscopy[46], aggregation-induced emission luminogen[47], cavity enhanced Raman scattering and laser induced fluorescence[43].

Regarding the vapor transfer into an evaporating drop, Seaver *et al.* reported on the condensation of water onto an evaporating butanol drop for the first time[48]. Using optical microscopy, they studied the evaporation of acoustically levitated butanol drops. Two different evaporative regimes were identified. Initially, evaporation proceeds following a similar trend to that of pure butanol and thereafter, similar to that of pure water evaporating in humid air. Smolík and Schwarz also observed condensation, in this case of naphthalene, onto water drops evaporating in air-steam-naphthalene atmosphere[49]. The condensation of supercooled naphthalene was supported by heterogeneous nucleation theory. More recently, Persad *et al.* investigated the effect of single and multicomponent atmosphere on the evaporation of water, ethanol and methanol drops[50]. They found that temperature at the interface of a drop evaporating in a multicomponent atmosphere, *i.e.* water and ethanol atmosphere, pulsates/oscillates due to the energy released from adsorption-absorption of the second component onto the drop. On the other hand, no oscillations were reported when evaporating in its own vapor.

The effect of the surrounding atmosphere (temperature and relative humidity) on mass and energy transport of ethanol drops undergoing evaporation was also investigated by means of infrared (IR) thermography [17]. The decrease in the strength of the hydrothermal patterns and the number of hydrothermal waves (HTWs) due to water adsorbing-absorbing and/or condensing onto the interface was reported. These observations were in agreement with previous work of Innocenzi *et al.*, where water condensation onto ethanol and ethanol-water drops was monitored by means of time-resolved infrared spectroscopy[51]. Moreover, by looking into the drop

evaporative behavior, *i.e.*, drop shape, Liu *et al.* also inferred the condensation of ethanol onto pure water and ethanol-water drops evaporating in an ethanol saturated atmosphere[52]. They concluded that in the case of binary mixtures, water condensation is driven by the decrease in the water vapor pressure at the liquid-vapor interface when compared to pure water. More recently, Chen *et al.* coupled acoustic and infrared approaches to estimate the concentration of ethanol and butanol at the drop bottom and at the drop interface, respectively, during the evaporation of ethanol-water and butanol-water mixtures[53].

In spite of the above mentioned investigations, none of these studies presented accurate and direct quantification of the drop composition in time, which could assist in a more detailed description of the coupling between heat and mass transfer during organic drops evaporation. In addition, purity of the solvent might be affected by the here mentioned phenomena. Hence, to further understand the effect of vapor transfer into evaporating organic solvent drops, we present the first direct quantitative analysis of the composition of ethanol drops evaporating in humid air at different ambient temperatures and relative humidity. A CCD camera and subsequent analysis with Matlab® enabled the extraction of the drop profile (base radius, contact angle and volume) in time. Drop composition at different stages of evaporation was then analyzed with Gas Injection Chromatography (GIC). The amount of water adsorbed-absorbed and/or condensed and that of ethanol evaporated is then quantified at different stages of evaporation by combining drop composition with drop profile. In addition, IR thermography was used to track the drop temperature profile at the liquid-gas interface. The greater ethanol evaporation rates observed at high temperatures and at high relative humidity are supported by diffusion limited evaporation model while the greater adsorption-absorption and/or condensation is demonstrated by heterogeneous nucleation theory. We conclude that at low relative humidity the main governing mechanism for water intake is that of adsorption-absorption, whereas at high relative humidity condensation plays a more relevant role. In addition, to predict the evaporative behavior of such

drops, we propose a combined evaporation-absorption/adsorption and/or condensation empirical correlation. The proposed correlation is based on the diffusive evaporative model that accounts for the decreases in ethanol concentration within the drop as well as for the water adsorption-absorption and/or condensation, and for the diffusion coefficient dependence on the ambient relative humidity. The proposed correlation agrees remarkably well with the experimental observations.

Experimental Procedures

Experiments were carried out in a PR-3KT environmental chamber from ESPEC Corp. (USA) where ambient temperature (T_{amb}) and relative humidity (RH) can be finely controlled between 10 °C and 85 °C and from 20% to 90%, respectively. In addition, a Type K thermocouple was placed inside the chamber to confirm the temperature displayed by the environmental chamber, which showed differences within ± 1 °C. A CCD camera Sentech STC-MC152USB with a Cosmicar TV Zoom lens and a back light were used to capture the evolution of the drop profile in time. Thereafter, drop volume, V (µl), radius, R (mm), and contact angle, θ (deg), were extracted in time, t (seconds), using Matlab® and assuming spherical cap[17]. A 9.5 x 9.5 x 1 mm^3 copper plate coated with a thin layer of CYTOP (C-C, C-F and C-O perfluorinated polymer) was used as substrate. We note here that CYTOP coating was applied to the copper to ensure more reproducible spherical drops[17]. 99.5% ethanol was purchased from Kanto Chemical Co. (Japan). An IR camera SC4000 from FLIR (USA) with spectral range between 3 and 5 µm was used to capture the drop temperature at the liquid-gas interface. A schematic of the experimental setup is shown in Figure 1a. The chamber precision range of environmental conditions as reported by the manufacturer is presented in Figure 1b. The experimental conditions (T_{amb}, RH) studied are included in Figure 1b&c.

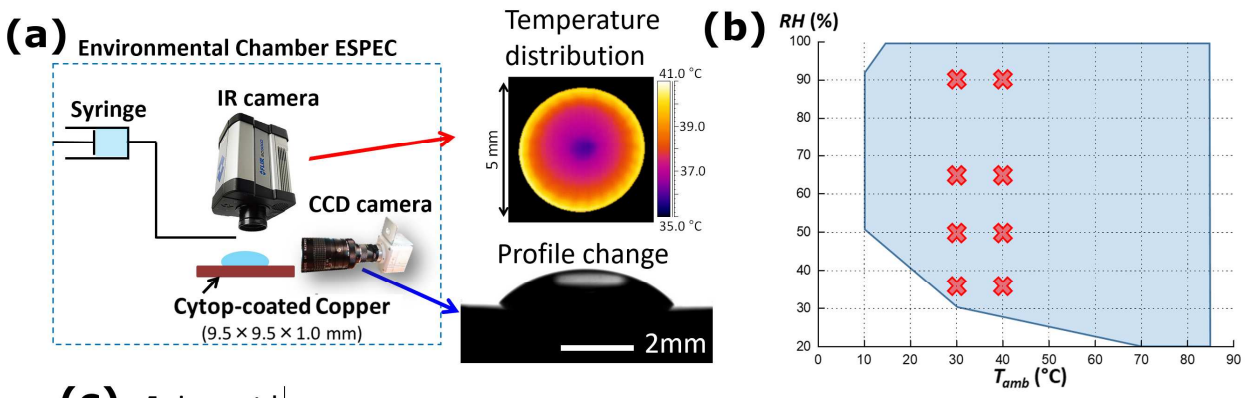

(c)

Environmental Conditions (T_{amb}, RH)	30 °C, 35%	30 °C, 50%	30 °C, 65%	30 °C, 90%	40 °C, 35%	40 °C, 50%	40 °C, 65%	40 °C, 90%
Dew Temperature (T_{dew})	13 °C	19 °C	23 °C	29 °C	21 °C	27 °C	32 °C	38 °C

Figure 1 - (a) Schematic of the experimental setup including: environmental chamber, syringe and dosing system, copper substrate coated with CYTOP, infrared and CCD cameras. IR snapshot of an evaporating ethanol drop from the top and CCD camera snapshot from the side are also included. (b) In solid blue, range of the environmental chamber as ambient temperature, T_{amb}, versus relative humidity, RH. Red crosses represent the experimental conditions studied in this work. (c) Environmental conditions studied as T_{amb}, RH and equivalent dew temperature, T_{dew}, for each condition.

The experimental procedure is described next. Firstly, to ensure homogeneous temperature between the ambient, the fluid and the substrate, T_{amb} and RH are set for 30 minutes. Next, CCD and IR cameras are triggered and the evolution of the drop profile and drop interface temperature are recorded at 4.8 fps and 5 fps, respectively. Before drop deposition, the chamber is turned off to avoid any interference due to vibrations. A drop of *ca*. 7 µl is gently deposited on the substrate. We note here that due to the short duration of the experiments, environmental conditions exhibited minor fluctuation within ± 1 ºC T_{amb} and ± 5% RH. We note here that change in the saturation concentration of ethanol at the droplet interface and hence on the ethanol evaporation due to fluctuations in the environmental conditions within the chamber is within 5%, which can be considered within the experimental observations deviation. In addition, change in the amount

of water adsorbed-absorbed and/or condensed from GIC is also estimated within 5%, which is in the same order as the *RH* variation.

For the analysis of the drop composition, a 0.5 µl Hamilton^{TM} syringe with a needle with inside and outside diameter of 0.104 and 0.515 millimeters, respectively, is used to extract the liquid from the drop at different stages of evaporation as represented in Figure 2a. A x-y-z axis micrometer manual translation stage from Sigma Koki (Japan) is used to guide the insertion of the needle into the drop for liquid extraction at different evaporating times and at different environmental conditions studied with minimal interfacial disruption during extraction. We note here that each GIC data corresponds to the average of three independent drop evaporation experiments. 0.2 ± 0.1 microliter are extracted from the drop for each condition, taken to a Gas Injection Chromatograph (GIC) GC-2010 Plus from Shimadzu (Japan) and analyzed (Figure 2b&c). We must note here that 50% error reported on sample extraction did not affect the GIC composition analysis or the results on droplet evaporation behavior since each GIC data point corresponds to the average of three independent drop evaporation experiments without intermediate sample extraction. In addition, GIC requires ca. 1 µg of injection sample compared to the 200 µg extracted, hence the amount needed for analysis can be considered negligible compared to the amount of volume extracted and its associated error. A schematic representation of the procedure for drop deposition and liquid extraction (Figure 2a), picture of the GIC (Figure 2b), intensity peaks obtained from the GIC versus retention time (Figure 2c), and calibration curve for the ethanol volume concentration (%) versus $A_{ethanol\ peak}$ / $A_{total\ peaks}$ at T_{amb} = 30 °C (Figure 2d) are represented in Figure 2:

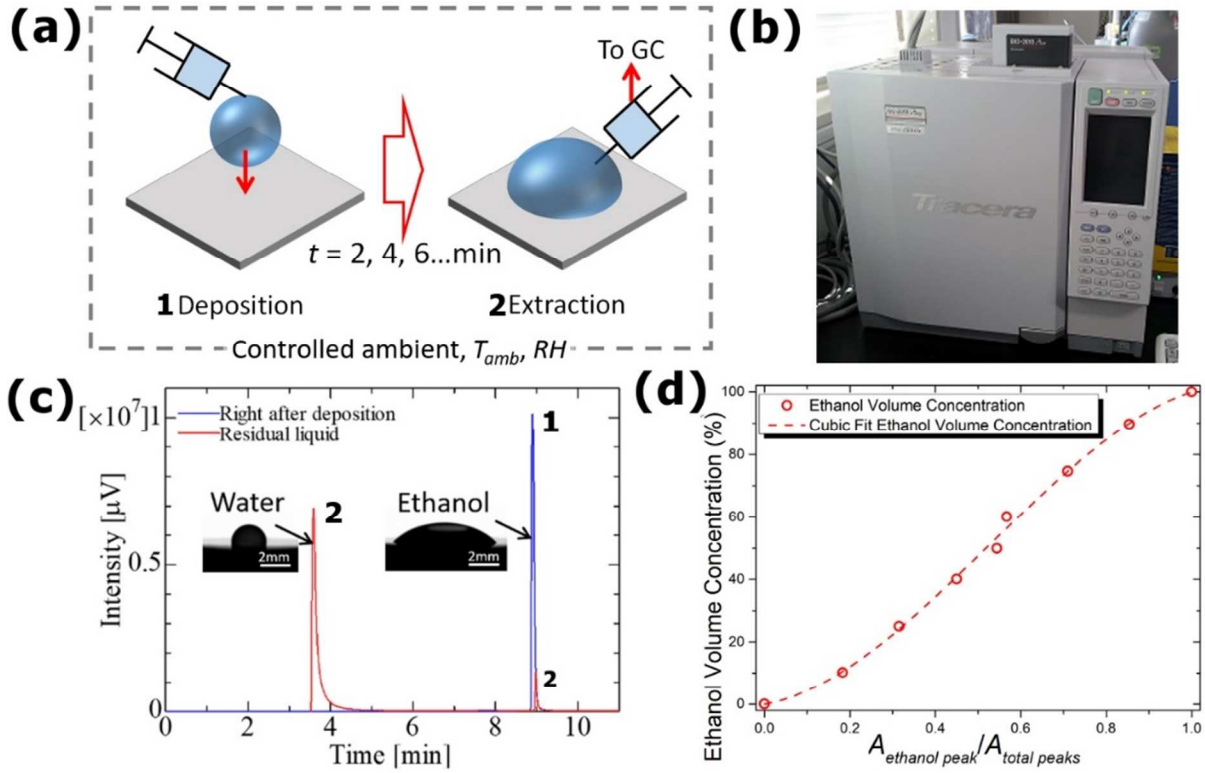

Figure 2 – (a) Schematic representation of drop deposition (stage 1) and liquid extraction (stage 2), (b) picture of the GIC Shimadzu GC-2010 Plus, (c) intensity (μV) versus retention time (min) at stage 1 (right after deposition) and stage 2 (after some evaporation) obtained from GIC analysis, and (d) GIC calibration curve for the ethanol volume concentration (%) versus ratio ethanol peak area to total peaks area, $A_{ethanol\ peak}$ / $A_{total\ peaks}$, at T_{amb} = 30 °C. Cubic fitting is included for comparison. We note here that the trend for T_{amb} = 40 °C is nearly the same.

Right after ethanol drop deposition, GIC analysis in Figure 2c only shows one intensity peak at *ca.* 9 minutes which corresponds to pure ethanol. However, after a certain evaporation time, two distinctive peaks can be observed in Figure 2c: one peak at *ca.* 9 minutes and a new peak appears at *ca.* 4 minutes, which are attributed to ethanol and to water, respectively. To obtain the ethanol volume concentration (%) from the GIC intensity data, calibration of the GIC was carried out prior to drop evaporation experiments. Pure ethanol, pure water and seven different intermediate concentrations of ethanol-water mixtures at T_{amb} = 30 °C and at T_{amb} = 40 °C were prepared and analyzed with the GIC. For each of the ethanol-water mixtures, the ratio of area of ethanol peak to the total area of ethanol and water peaks, $A_{ethanol\ peak}$ / $A_{total\ peaks}$,

was calculated from the intensity versus retention time data. Then, the ethanol volume concentration versus $A_{ethanol\ peak}$ / $A_{total\ peaks}$ can be plotted in Figure 2d. From Figure 2d, the ethanol volume concentration versus $A_{ethanol\ peak}$ / $A_{total\ peaks}$ closely follows a relatively linear trend.

Results and Discussion

Drop Profile Evaporative Behavior

In what follows we present representative experimental observations of ethanol drops evaporating on a copper substrate coated with a thin layer of CYTOP. The evolution of contact angle, θ, contact radius, R, height, h, and volume, V, versus time, t, for T_{amb} = 30 °C and T_{amb} = 40 °C at different RH are included in Figure 3. We note here that no liquid extraction for GIC analysis was carried out during the experimental observations presented in Figure 3.

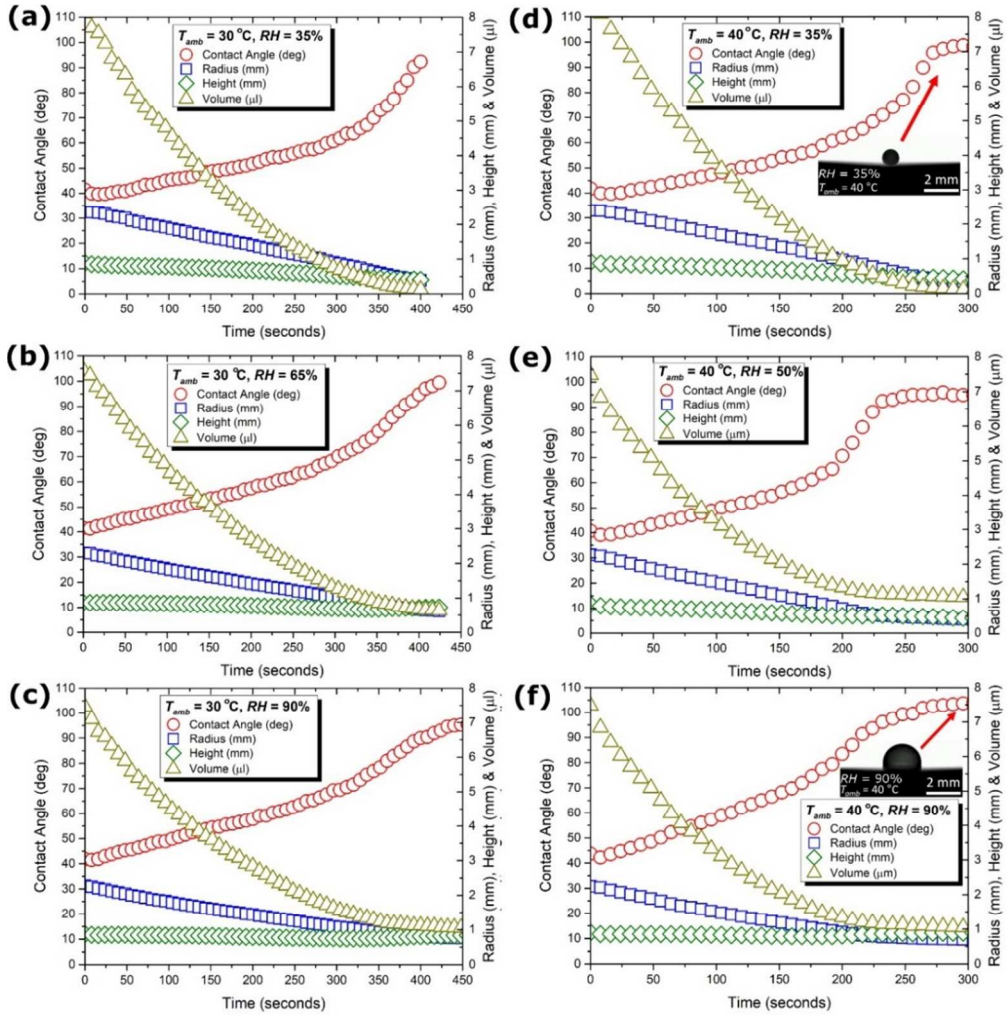

Figure 3 – Representative evaporative behavior as evolution of (circles) contact angle, θ (deg), (squares) contact radius, R (mm), (diamonds) height, h (mm), and (up-triangles) volume, V (µl), versus time, t (seconds), for (a) T_{amb} = 30 °C - RH = 35%, (b) T_{amb} = 30 °C - RH = 65%, (c) T_{amb} = 30 °C - RH = 90%, (d) T_{amb} = 40 °C - RH = 35%, (e) T_{amb} = 40 °C - RH = 50%, and (f) T_{amb} = 40 °C - RH = 90%. Insights of (d) and (f) show the drop shape after most of the ethanol evaporates. We note that for better representation we have reduced the number data points by a factor of 20.

From Figure 3, qualitatively the evaporative behavior is very similar for all environmental conditions. After the drop deposition, the base radius monotonically decreases until the last instants of evaporation where it remains practically constant. On the other hand, the contact angle decreases for the initial 10 seconds of the evaporation and thereafter increases until it reaches a plateau at *ca.* 100°. The initial decrease in contact angle is attributed to the loss of ethanol during evaporation, whereas the increase in contact angle is ascribed to the increase in the water concentration at the liquid-gas interface and within the drop. Due to the water adsorbed-absorbed and/or condensed, the final shape of the drop tends to that of pure water on a low surface energy surface[54].

As a consequence of the interplay between ethanol evaporation and water adsorption-absorption and/or condensation, the evolution of the drop volume in time follows a decreasing quadratic form followed by a plateau. It is worth noting that at high ambient temperature (T_{amb} = 40 °C), the volume reaches a plateau earlier than at low ambient temperature (T_{amb} = 30 °C). Also we stress here that the final drop volume is greater with increasing *RH*. The drop height usually decreases at low *RH*, whereas it remains fairly constant for half of the drop lifetime followed by an increase to account for the change in contact angle at high *RH*. In view of this unique evaporative behavior it is reasonable to emphasize that as ethanol evaporates and water adsorbs-absorbs and/or condenses, the composition of the water drop transitions from pure ethanol to pure water[17, 52]. Due to water being adsorbed-absorbed and/or condensed, the evaporative behavior does not follow any of the well-known evaporation modes previously reported in literature: the constant contact radius[55], the constant contact angle[55] or the mixed mode[56, 57]. Here

we report a mixed evaporation-adsorption-absorption and/or condensation mode where the contact radius decreases monotonically while the contact angle increases.

Infrared Thermography Behavior

Figure 4 includes representative raw IR temperature snapshots at the drop liquid-gas interface for T_{amb} = 40 °C at 35% and at 90% *RH* at different evaporating times.

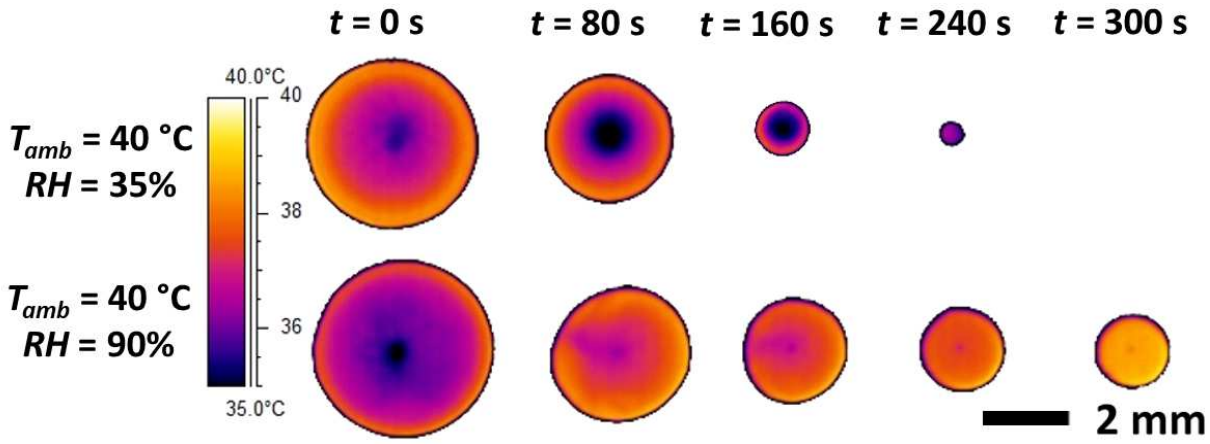

Figure 4 – Raw IR snapshots of the drop liquid-gas interface at T_{amb} = 40 °C and (up) *RH* = 35% and (down) *RH* =90% at *t* = 0, 80, 160, 240 and 300 seconds. Color scale bar represents temperature distribution from 35 °C (dark-blue) to 40 °C (bright-yellow). Scale bar is 2 mm.

From Figure 4, the decrease in drop size, *i.e.*, decrease in drop radius, in time is evident. At low *RH* the drop radius monotonically shrinks until the drop completely evaporates, whereas at high *RH* the drop radius decreases and then reaches a plateau for several minutes where the drop seems to not evaporate further. This behavior is consistent with the evolution of the drop radius presented earlier in Figure 3. When looking into IR thermography data (Figure 4), as ethanol evaporates the temperature at the drop interface decreaes due to evaporative cooling. Part of the latent heat of evaporation is removed from the drop and, as a consequence, the drop interfacial temperature decreases below that of the ambient ($T_{interface} < T_{amb}$). A temperature

gradient appears at the drop interface giving rise to self-generated HTWs that induce mixing within the drop (Figure 4)[17, 58]. At low *RH*, there is stronger evaporative cooling and hence stronger mixing than at high *RH* (Figure 4a vs. Figure 4b). At high *RH* the heat of water adsorption-absorption and/or condensation keeps the drop temperature more uniform hindering evaporative cooling effect.

Gas Injection Chromatography

To directly quantify the amount of water adsorbed-absorbed and/or condensed during ethanol drop evaporation, Figure 5 shows GIC experimental results as ethanol volume concentration (%) in time at T_{amb} = 30 °C and T_{amb} = 40 °C and 25%, 50% and 90% *RH*. Figure 5 represents the first systematic direct quantification of the composition in time of evaporating ethanol drops.

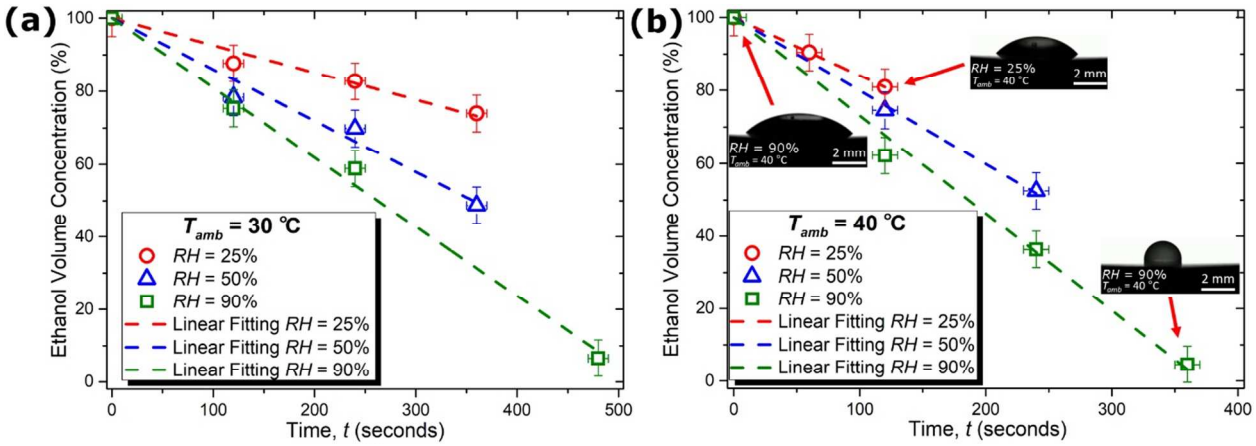

Figure 5 – Ethanol volume concentration (%) versus time, *t* (sec), for ethanol drops evaporating in a controlled atmosphere at (a) T_{amb} = 30 °C and (b) T_{amb} = 40 °C for (triangles) 25%, (squares) 50% and (circles) 90% *RH*. The remaining concentration is that of water (x_{water} = 1 - $x_{ethanol}$). Each data point shows the average of 3 independent experiments with standard deviation ± 5% and ± 10 seconds for the ethanol volume concentration and for the drop lifetime, respectively. Linear fitting is included to illustrate the trend. For T_{amb} = 40 °C the drop profile before extraction at *t* = 0

seconds, and after extraction at t = 120 seconds for RH = 25% and at t = 360 seconds for RH = 90% are also included along.

Figure 5 shows that the concentration of ethanol decreases quasi-linearly with time while the volume concentration of water increases accordingly (water volume concentration = 100% – ethanol volume concentration: $x_{water} = 1 - x_{ethanol}$) for any of the conditions studied. The decrease in the ethanol volume concentration is attributed to the simultaneous coupling mechanisms of ethanol evaporation and water adsorption-absorption and/or condensation. At high RH, a more rapid decrease in ethanol concentration is observed at both T_{amb} = 30 °C and T_{amb} = 40 °C, attributed to water condensation since the drop liquid-gas interface temperature decreases below that of T_{dew}. In addition, ethanol concentration decreases faster at high T_{amb} as expected, since both the diffusion coefficient and the vapor pressure of ethanol are proportional to temperature.

Nonetheless, GIC concentration data presented in Figure 5 does not directly account for the amount of ethanol evaporating and/or for the amount of water adsorbed-absorbed and/or condensed. To be able to interpret and compare the amount of ethanol evaporated and the amount of water adsorbed-absorbed and/or condensed, we combine drop profile just before sample extraction obtained from CCD images (Figure 3) with the quantitative information of the volume concentration retrieved from GIC (Figure 5). Quantification of ethanol and water volume evolution over time is then represented in Figure 6. For simplicity, we represent the volume of ethanol and that of water normalized by the initial drop volume. We must mention here that due to the polar nature of both water and ethanol, a mixture ethanol-water typically shows a 1.2% decrease in volume at 40%-60% ethanol-water molar concentration when compared to the pure liquids. However, such change in volume can be considered negligible and within the experimental error reported[59].

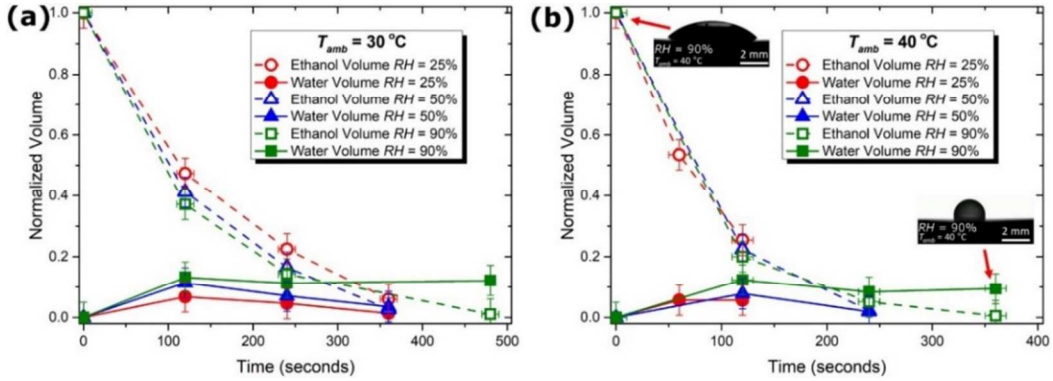

Figure 6 – (empty symbols) Normalized volume of ethanol and (filled symbols) normalized volume of water with respect to the initial drop volume versus time, *t* (sec), for (circles) 25%, (triangles) 50% and (squares) 90% *RH* at (a) T_{amb} = 30 °C and (b) T_{amb} = 40 °C. Solid lines and dashed lines connecting the different data points are included to illustrate the water and ethanol trends, respectively.

From Figure 6, the continuous decrease in the amount of ethanol in time is reported, which is consistent with the works of Innocenzi *et al.*[51] and Liu *et al.*[52]. The presence of water within the drop is also in agreement with the changes in absorbance due to water absorption onto an evaporating ethanol drop as reported by Innocenzi *et al.*[51]. From Figure 6, it is also worth noting the presence of residual ethanol in the last stage of evaporation, which is consistent with the findings of Sefiane *et al.* and Li *et al.*[44, 52]. Residual ethanol present at the last stage of the drop evaporation is attributed to the slow diffusion of the ethanol from the bulk of the drop towards the liquid-gas interface. It is worth noting here that the continuous mixing induced by HTWs at early stages of evaporation shall keep a more uniform ethanol and water concentrations within the drop, whereas at later stages of evaporation an ethanol concentration gradient may develop due to the absence of HTWs mixing[17, 52]. In addition, the more rapid evaporation of ethanol at high temperatures, *i.e.*, T_{amb} = 40 °C (Figure 5b) when compared to T_{amb} = 30 °C (Figure 5a), is also reported. When looking into water adsorbed-absorbed and/or condensed,

greater amount of water is found at high *RH*, whereas no major differences are found when comparing the total amount of water intake for different T_{amb}.

Evaporation-Absorption/Adsorption and/or Condensation Empirical Model

Next, to account for the different evolutions of drop volume in time due to the coupling mechanisms of ethanol evaporation and that of water adsorption-absorption and/or condensation, we then propose a combined evaporation-absorption/adsorption and/or condensation empirical model to capture the experimental observations reported. The drop evaporation rate is estimated using Popov's evaporative model for a moving contact line from the work of Stauber *et al*. as[60-62]:

$$\frac{\mathrm{d}V}{\mathrm{d}t} = -\frac{\pi D_{12}(T_{amb})\,(c_{sat}(T_{amb}) - c_{\infty})}{\rho}\,\frac{R\,g(\theta)}{(1+\cos\theta)^2} \qquad \text{Eq.1}$$

where $\mathrm{d}V/\mathrm{d}t$ is the change of volume in time or evaporation rate, R and θ are the drop radius and contact angle changing in time, ρ is the density, c_{sat} and c_{∞} are the saturation concentration of ethanol and the concentration of ethanol far away from the drop ($c_{\infty} = 0$), and D_{12} is the diffusion coefficient of 1 in 2, in this case of ethanol in water[63, 64]. Both D_{12} and c_{sat} are proportional to the ambient temperature T_{amb}. c_{sat} is considered to change linearly with temperature according to the following relation $c_{sat}(T) = c_{sat}(T_{amb}) + \left.\mathrm{d}c_{sat}/\mathrm{d}T\right|_{T=T_{amb}} (T - T_{amb})$[65] and D_{12} is proportional to temperature as $D_{12} \propto T^{3/2}$[66, 67]. At high T_{amb}, the larger ethanol c_{sat} at the interface and greater D_{12} induce the faster ethanol evaporation reported (Figure 6a vs. Figure 6b). On the other hand, $g(\theta)$ is a function that accounts for the non-uniform diffusion along the drop interface and is given by;

$$g(\theta) = (1+\cos\theta)^2 \left\{ \tan\frac{\theta}{2} + 8\int_0^\infty \frac{\cosh^2\theta\tau}{\sin 2\pi\tau} \tanh[\tau(\pi-\theta)]\,d\tau \right\} \quad \text{Eq.2}$$

where τ is the normalized drop lifetime. Then, the evolution of the drop volume based on the diffusion model is estimated by making use of Equation 1and plotted in Figure 7 along with our own experimental results. By comparing experimental values to those estimated using Equation 1, the drop evaporation rate is clearly overestimated. Such overestimation is due to the fact that Equation 1 assumes c_{sat} (T_{amb}) as constant and only function on T_{amb}. However, from GIC experimental results (Figure 5), the ethanol concentration actually decreases in time. Hence, dV/dt must be proportional to the ethanol concentration at the liquid-gas interface as c_{sat} (T_{amb}) * $x_{\text{ethanol-int}}$, which is now accounted for in Equation 3:

$$\frac{dV}{dt} = -\frac{\pi D_{12}(T_{amb}) c_{sat}(T_{amb}) x_{ethanol-\text{int}}}{\rho} \frac{R\,g(\theta)}{(1+\cos\theta)^2} \quad \text{Eq.3}$$

We must note here that upon the adsorption-absorption and/or condensation the transition from pure ethanol to water induces; the local change in the temperature and composition at the microscopic liquid-gas interface, and the gradient of species concentration within the drop[43, 58]. Nonetheless, vigorous mixing induced both by the self-generating HTWs due to evaporative cooling[17, 68] and by the ethanol preferential evaporation for ethanol-water mixtures[41, 69] should in turn homogenize concentration the ethanol and water profiles within the drop. In addition, concentration profiles of an ethanol-water mixture evaporating did only show small change in the concentration profile at the liquid-vapor interface[70]. Hence at this stage it is reasonable to assume $x_{\text{ethano-int}}$ as x_{ethanol} as extracted from GIC.

Results obtained by making use of Equation 3 remarkably agree albeit qualitatively with the experimental evolution of the drop volume in time as shown in Figure 7. Only in the case of T_{amb} = 30 °C and RH = 35% the evaporation rate is underestimated and as a consequence the volume

predicted is larger than the one reported experimentally. In the case of T_{amb} = 30 °C and RH = 65% and T_{amb} = 30 °C and RH = 90% the quantitative agreement is remarkable. On the other hand, for T_{amb} = 40 °C the evaporation rate is overestimated at later stages of evaporation. We note here that although other works stress the importance to account for the gradient of concentration between the bulk and the interface,[70] our assumption of assuming a homogeneous concentration of ethanol and water within the drop is rather reasonable due to the presence of internal mixing induced by the observed HTWs[17, 68] and by the expected preferential ethanol evaporation[41].

When considering the diffusion coefficient,D_{12} is inversely proportional to the molecular mass of the respective diffusing elements: $D_{12} \propto (1/M_1 + 1/M_2)^{0.5}$ [66, 67]. Since the density of humid air is lower than that of dry air, then, by making use of the law of ideal gases, the molecular mass of wet air is found to be smaller when compared to that of dry air[71, 72]. Then, water vapor being lighter than air, convection in the gas phase in the vicinity of the drop interface is induced, which can further enhance mass transfer[65, 73]. Then, assuming that the temperature of the gas phase does not change and that D_{12} is function of RH as: $D_{12} \propto D_{12}(T_{amb}, RH)$, we can rewrite Equation 3 as:

$$\frac{dV}{dt} = -\frac{\pi D_{12}(T_{amb}, RH) c_{sat}(T_{amb}) x_{ethanol}}{\rho} \frac{Rg(\theta)}{(1+\cos\theta)^2} \qquad \text{Eq.4}$$

By plotting the drop volume using Equation 4 along with experimental results from the present study (Figure 7), small differences can be discerned when comparing to Equation 3. This is due to the small change in the diffusion coefficient due to the difference in relative humidity. The excellent qualitative agreement reported for all environmental conditions as for Equation 3 prevails. Nonetheless, both Equation 3 and Equation 4 are not able to fully, quantitatively,

capture the evolution of the volume in time at T_{amb} = 40 °C. At this point, we must take into account the water adsorbing-absorbing and/or condensing in time. Then an additional term to account for the water intake must be added to Equation 4. From Figure 5 we can assume the increase in water concentration, x_{water}, as being linear with time and equal to 1-x_{ethanol} or following a linear relation as A t. Then Equation 4 is rewritten as Equation 5 below:

$$\frac{dV}{dt} = -\frac{\pi D_{12}(T_{\text{amb}}, RH) c_{sat}(T_{amb}) x_{ethanol}}{\rho} \frac{Rg(\theta)}{(1+\cos\theta)^2} + \frac{dx_{water}}{dt} V \qquad \text{Eq.5}$$

By accounting for the water absorbed-adsorbed and/or condensed, the drop volume over time is greater than that predicted by Equation 4. Such an increase in volume is more marked for high relative humidity cases as expected. When comparing our experimental results to those predicted by Equation 5, there is a remarkable qualitative and quantitative agreement when accounting for: the simultaneous ethanol evaporation and water intake. In the case of T_{amb} = 30 °C, the greater experimental evaporation rates observed can be attributed to both convection within the drop and in the vapor phase.[74-76] We note here that for the precise prediction of the evaporation rate, convection within the drop and within the atmosphere, as well as using the interfacial temperature of the drop rather than that of the ambient for the calculations of c_{sat} must be accounted for.

Figure 7 includes experimental drop volume in time, and predicted drop volumes by Popovs' model (Equation 1), by accounting for the decrease of ethanol concentration in time (Equation 3), by taking into account the diffusion coefficient function of *RH* (Equation 4) and by taking into account the water absorbed-adsorbed and/or condensed (Equation 5):

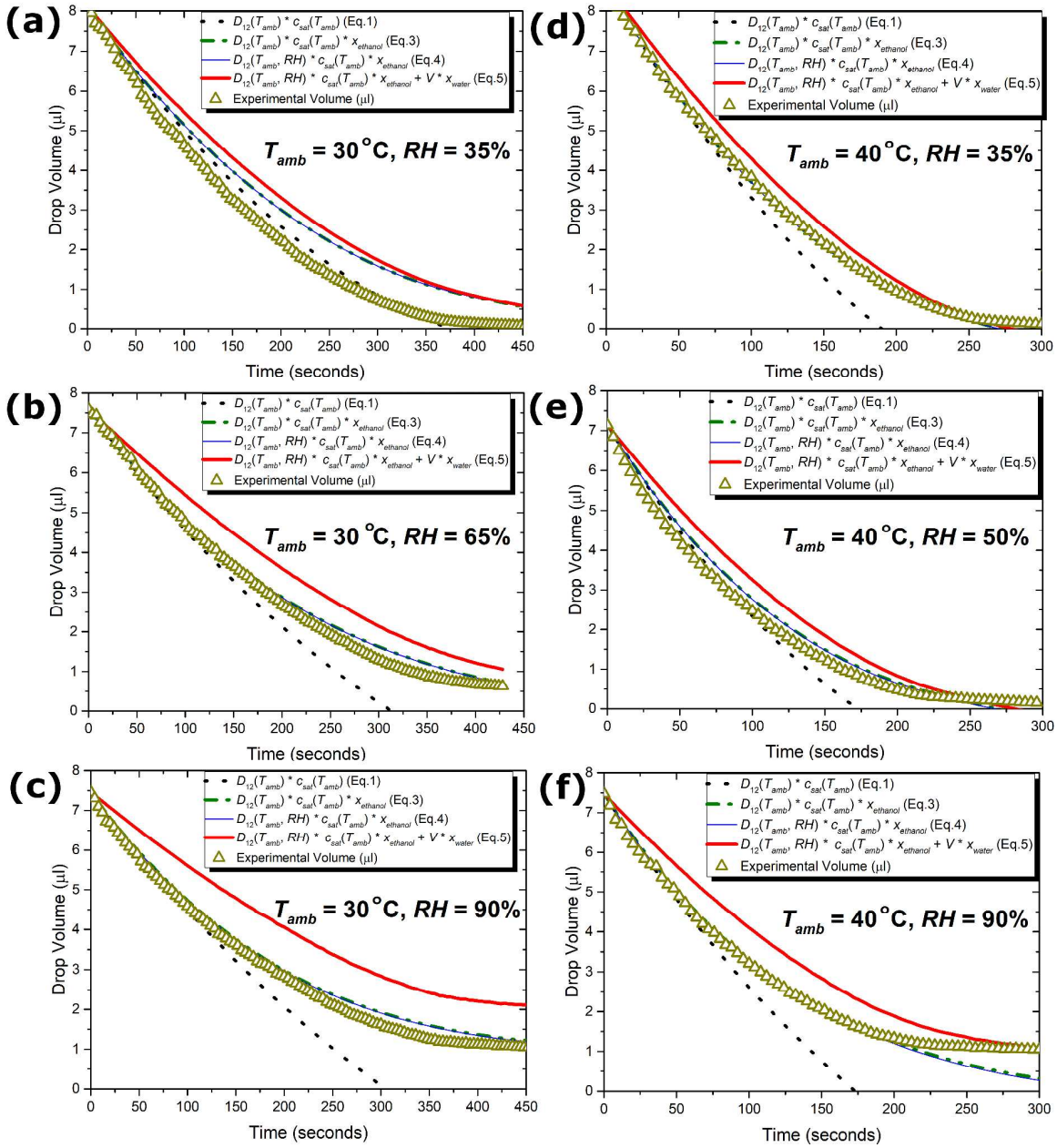

Figure 7 – Evolution of drop volume, V (µl), versus time, t (seconds), for (a) T_{amb} = 30 °C - RH = 35%, (b) T_{amb} = 30 °C - RH = 65%, (c) T_{amb} = 30 °C - RH = 90%, (d) T_{amb} = 40 °C - RH = 35%, (e) T_{amb} = 40 °C - RH = 50% and (f) T_{amb} = 40 °C - RH = 90%. (up-triangles) Experimental evaporative trend, (dotted line) diffusive evaporation model as in Eq.1, (dashed-dotted line) accounting for $c_{sat}(T_{amb})*x_{ethanol}$ as in Eq.3, (thin-solid line) accounting for $c_{sat}(T_{amb})*x_{ethanol}$ as in Eq.4, and (thick-solid line) accounting for $c_{sat}(T_{amb})*x_{ethanol}$ and water absorbed-adsorbed and/or condensed ($V * x_{water}$) as in Eq.5.

The model proposed remarkably captures both qualitatively and quantitatively the dynamic evolution of the drop volume within less than 20% deviation from the initial drop

volume. Despites the good agreement between empirical correlation proposed and experimental observations, further insights on the microscopic/dynamical origin of ethanol evaporation as water adsorbs-absorbs and/or condenses will be sought in future work.

In addition, we include further discussion to address the effect of relative humidity on ethanol drops. At high *RH*, T_{dew} (represented in Figure 1c) approaches that of T_{amb}, then as ethanol evaporates, due to evaporative cooling the temperature at the drop interface decreases below T_{dew} and hence condensation takes place. The greater amount of water adsorbed-absorbed and/or condensed at high *RH* is in agreement with heterogeneous classical nucleation theory, where the nucleation rate for condensation, *J*, can be expressed as[77]:

$$J = \frac{b\,P(4\pi R^{*2})n}{\sqrt{2\pi M k T}} \exp\left(-\frac{\Delta G^{*}}{k T}\right) \qquad \text{Eq.6}$$

where *P* and *T* are the pressure and temperature of the gas, R^{*} and ΔG^{*} are the critical radius and the free energy of nucleation, *k* is the Boltzmann constant, *b* is a constant and *n* is the gas number density. At high *RH*, the concentration of water molecules in the vicinity of the ethanol drop interface is greater, hence *n* is greater. For high *n*, there is higher probability for the molecules to reach the ethanol drop interface and condense. The greater water condensation at high *RH* is then demonstrated by heterogeneous classical nucleation theory. As time progresses, a maximum volume of water is reported at 20-30% of the drop lifetime, which is qualitatively consistent with the work of Innocenzi *et al.*[51]. Thereafter, in the case of low relative humidity, *i.e.*, $RH < 60\%$, the volume of water decreases, whereas in the case of $RH = 90\%$, the amount of water remains almost constant. We state here that at low *RH*, the main governing mechanism of water intake is that of adsorption-absorption, whereas at high *RH* water condensation is more prominent.

We conclude that our revisited evaporation rate empirical correlation accounting for: the change of ethanol concentration, the change in the diffusion coefficient function of the relative

humidity and the water intake in time, agrees remarkably with the experimental observations. In addition, we stress on the importance of accounting for the water vapor present in the environment for applications where the purity of the solvent is of paramount importance such as: medical diagnosis, DNA patterning, inkjet printing or materials processing.

Conclusions

A systematic direct quantitative analysis of composition in time of evaporating ethanol drops at different ambient temperatures and relative humidity has been undertaken. The volume of ethanol is found to decrease with time at all ambient temperatures and relative humidities. At high ambient temperature, the evaporation of ethanol is enhanced, since the diffusion coefficient and ethanol saturation concentration are proportional to temperature. Furthermore, we also report that ethanol evaporation is enhanced at high relative humidity, which is rationalized by the greater gas diffusion coefficient in the case of humid air when compared to that of dry air. On the other hand, as ethanol evaporates, water adsorbs-absorbs and/or condenses, which is also directly quantified in this work. At high relative humidity, the temperature at the drop interface falls below the dew point due to evaporative cooling and condensation takes place. Whereas at low relative humidity, the main governing mechanism for water intake onto the ethanol drop is that of adsorption-absorption. In addition, by looking into the heterogeneous classical nucleation theory, we argue that the greater amount of water molecules present in the vicinity of the drop interface at high relative humidity induces the greater probability for adsorption-absorption and/or condensation, which is demonstrated by the greater amount of water intake reported at high relative humidity. We then proposed a revisited empirical correlation for the evaporation of ethanol drops that accounts for; the change of ethanol concentration, the diffusion coefficient dependence on relative humidity and the water intake in time. The proposed correlation agrees

remarkably well with the experimental observations. To conclude, we stress the importance of humidity presence in the atmosphere to couple the heat and mass transfer during drop evaporation for the accurate modeling and prediction of organic solvents evaporation.

Acknowledgements

The authors acknowledge the support received from the International Institute for Carbon-Neutral Energy Research (WPI-I^{2}CNER) from the World Premier Research Center Initiative established by the Japanese Ministry of Education, Culture, Sports, Science and Technology (MEXT). Y.T. acknowledges the support received from JST-CREST. D.O. acknowledges the support received from the Japanese Society for the Promotion of Science (JSPS) KAKENHI (Grant no. JP16K18029 and JP18K13703).

Reference

1. P. G. de Gennes, *Reviews of Modern Physics*, 1985, **57**, 827-863.
2. K. S. Birdi and D. T. Vu, *Journal of Adhesion Science and Technology*, 1993, **7**, 485-493.
3. R. Bhardwaj, J. P. Longtin and D. Attinger, *International Journal of Heat and Mass Transfer*, 2007, **50**, 2912-2923.
4. S. David, K. Sefiane and L. Tadrist, *Colloids and Surfaces A: Physicochemical and Engineering Aspects*, 2007, **298**, 108-114.
5. J. L. Plawsky, M. Ojha, A. Chatterjee and P. C. Wayner, *Chemical Engineering Communications*, 2008, **196**, 658-696.
6. D. Bonn, J. Eggers, J. Indekeu, J. Meunier and E. Rolley, *Reviews of Modern Physics*, 2009, **81**, 739-805.
7. B. Sobac and D. Brutin, *Physical Review E*, 2012, **86**, 021602.
8. G. F. Harrington, J. M. Campbell and H. K. Christenson, *Crystal Growth & Design*, 2013, **13**, 5062-5067.
9. K. A. Baldwin and D. J. Fairhurst, *Soft Matter*, 2015, **11**, 1628-1633.
10. H. G. Houghton, *Journal of Applied Physics*, 1933, **4**, 419-424.
11. N. A. Fuchs, *Evaporation and Droplet Growth in Gaseous Media*, Pergamon Press, New-York, London, Oxford, Paris1959.
12. R. Taylor and R. Krishna, *Multicomponent Mass Transfer*, Wiley1993.
13. K. Sefiane, S. K. Wilson, S. David, G. J. Dunn and B. R. Duffy, *Physics of Fluids*, 2009, **21**, 062101.
14. A.-M. Cazabat and G. Guena, *Soft Matter*, 2010, **6**, 2591-2612.

15. D. Orejon, M. E. R. Shanahan, Y. Takata and K. Sefiane, *Langmuir*, 2016, **32**, 5812-5820.
16. H.-J. Butt, D. S. Golovko and E. Bonaccurso, *The Journal of Physical Chemistry B*, 2007, **111**, 5277-5283.
17. Y. Fukatani, D. Orejon, Y. Kita, Y. Takata, J. Kim and K. Sefiane, *Physical Review E*, 2016, **93**, 043103.
18. M. L. Shulman, R. J. Charlson and E. James Davis, *Journal of Aerosol Science*, 1997, **28**, 737-752.
19. H. Cha, A. Wu, M.-K. Kim, K. Saigusa, A. Liu and N. Miljkovic, *Nano Letters*, 2017, **17**, 7544-7551.
20. D. Orejon, K. Sefiane and Y. Takata, *Physical Review E*, 2014, **90**, 053012.
21. M. A. J. van Limbeek, P. B. J. Hoefnagels, C. Sun and D. Lohse, *Soft Matter*, 2017.
22. F. Celestini, T. Frisch and Y. Pomeau, *Soft Matter*, 2013, **9**, 9535-9538.
23. R. Bhardwaj, X. Fang, P. Somasundaran and D. Attinger, *Langmuir*, 2010, **26**, 7833-7842.
24. K. L. Maki and S. Kumar, *Langmuir*, 2011, **27**, 11347-11363.
25. S. Das, P. R. Waghmare, M. Fan, N. S. K. Gunda, S. S. Roy and S. K. Mitra, *RSC Advances*, 2012, **2**, 8390-8401.
26. V. Soulie, S. Karpitschka, F. Lequien, P. Prene, T. Zemb, H. Moehwald and H. Riegler, *Physical Chemistry Chemical Physics*, 2015, **17**, 22296-22303.
27. D. Willmer, K. A. Baldwin, C. Kwartnik and D. J. Fairhurst, *Physical Chemistry Chemical Physics*, 2010, **12**, 3998-4004.
28. D. Orejon, K. Sefiane and M. E. R. Shanahan, *Journal of Colloid and Interface Science*, 2013, **407**, 29-38.
29. S. Das, S. K. Mitra and S. Chakraborty, *Physical Review E*, 2012, **86**, 011603.
30. L. Espín and S. Kumar, *Physical Review Fluids*, 2017, **2**, 014004.
31. D. Pesach and A. Marmur, *Langmuir*, 1987, **3**, 519-524.
32. B. Jańczuk, T. Białopiotrowicz and W. Wójcik, *Journal of Colloid and Interface Science*, 1989, **127**, 59-66.
33. Y. Wen-Jei, K. H. Guo and T. Uemura, *International Journal of Heat and Mass Transfer*, 1989, **32**, 1197-1205.
34. S. M. Rowan, M. I. Newton, F. W. Driewer and G. McHale, *The Journal of Physical Chemistry B*, 2000, **104**, 8217-8220.
35. Y. Yonemoto and T. Kunugi, *International Journal of Heat and Mass Transfer*, 2016, **96**, 614-626.
36. P. P. Bag and C. M. Reddy, *Crystal Growth & Design*, 2012, **12**, 2740-2743.
37. H. Fan, Y. Lu, A. Stump, S. T. Reed, T. Baer, R. Schunk, V. Perez-Luna, G. P. López and C. J. Brinker, *Nature*, 2000, **405**, 56.
38. V. Dugas, J. Broutin and E. Souteyrand, *Langmuir*, 2005, **21**, 9130-9136.
39. N. H. Bhatt, Lily, R. Raj, P. Varshney, A. R. Pati, D. Chouhan, A. Kumar, B. Munshi and S. S. Mohapatra, *International Journal of Heat and Mass Transfer*, 2017, **110**, 330-347.
40. K. Sefiane, L. Tadrist and M. Douglas, *International Journal of Heat and Mass Transfer*, 2003, **46**, 4527-4534.
41. J. R. E. Christy, Y. Hamamoto and K. Sefiane, *Physical Review Letters*, 2011, **106**, 205701.
42. P. J. Sáenz, A. W. Wray, Z. Che, O. K. Matar, P. Valluri, J. Kim and K. Sefiane, *Nature Communications*, 2017, **8**, 14783.
43. R. J. Hopkins and J. P. Reid, *The Journal of Physical Chemistry A*, 2005, **109**, 7923-7931.
44. K. Sefiane, S. David and M. E. R. Shanahan, *The Journal of Physical Chemistry B*, 2008, **112**, 11317-11323.
45. S. Manukyan, H. M. Sauer, I. V. Roisman, K. A. Baldwin, D. J. Fairhurst, H. Liang, J. Venzmer and C. Tropea, *Journal of Colloid and Interface Science*, 2013, **395**, 287-293.
46. Z. Lu, M. H. K. Schaarsberg, X. Zhu, L. Y. Yeo, D. Lohse and X. Zhang, *Proceedings of the National Academy of Sciences*, 2017, **114**, 10332-10337.

47. X. Cai, N. Xie, Z. Qiu, J. Yang, M. He, K. S. Wong, B. Z. Tang and H. Qiu, *ACS Applied Materials & Interfaces*, 2017, **9**, 29157-29166.
48. M. Seaver, A. Galloway and T. J. Manuccia, *Aerosol Science and Technology*, 1990, **12**, 741-744.
49. J. Smolík and J. Schwarz, *Journal of Colloid and Interface Science*, 1997, **185**, 382-389.
50. A. H. Persad, K. Sefiane and C. A. Ward, *Langmuir*, 2013, **29**, 13239-13250.
51. P. Innocenzi, L. Malfatti, S. Costacurta, T. Kidchob, M. Piccinini and A. Marcelli, *The Journal of Physical Chemistry A*, 2008, **112**, 6512-6516.
52. C. Liu, E. Bonaccurso and H.-J. Butt, *Physical Chemistry Chemical Physics*, 2008, **10**, 7150-7157.
53. P. Chen, M. Toubal, J. Carlier, S. Harmand, B. Nongaillard and M. Bigerelle, *Langmuir*, 2016, **32**, 9836-9845.
54. D. Orejon, K. Sefiane and M. E. R. Shanahan, *Langmuir*, 2011, **27**, 12834-12843.
55. R. G. Picknett and R. Bexon, *Journal of Colloid and Interface Science*, 1977, **61**, 336-350.
56. C. Bourges-Monnier and M. E. R. Shanahan, *Langmuir*, 1995, **11**, 2820-2829.
57. P. J. Sáenz, K. Sefiane, J. Kim, O. K. Matar and P. Valluri, *Journal of Fluid Mechanics*, 2015, **772**, 705-739.
58. X. Qu, E. J. Davis and B. D. Swanson, *Journal of Aerosol Science*, 2001, **32**, 1315-1339.
59. D. W. Green and R. H. Perry, *Perry's Chemical Engineers' Handbook, Eighth Edition*, McGraw-Hill Education2007.
60. Y. O. Popov, *Physical Review E*, 2005, **71**, 036313.
61. A. A. Günay, S. Sett, J. Oh and N. Miljkovic, *Langmuir*, 2017, **33**, 12007-12015.
62. J. M. Stauber, S. K. Wilson, B. R. Duffy and K. Sefiane, *Physics of Fluids*, 2015, **27**, 122101.
63. H. Hu and R. G. Larson, *The Journal of Physical Chemistry B*, 2002, **106**, 1334-1344.
64. H. Hu and R. G. Larson, *Langmuir*, 2005, **21**, 3963-3971.
65. G. J. Dunn, S. K. Wilson, B. R. Duffy, S. David and K. Sefiane, *Journal of Fluid Mechanics*, 2009, **623**, 329-351.
66. N. H. Chen and D. F. Othmer, *Journal of Chemical & Engineering Data*, 1962, **7**, 37-41.
67. J. C. Slattery and R. B. Bird, *AIChE Journal*, 1958, **4**, 137-142.
68. X. Zhong and F. Duan, *Scientific Reports*, 2017, **7**, 16219.
69. R. Bennacer and K. Sefiane, *Journal of Fluid Mechanics*, 2014, **749**, 649-665.
70. S. Dehaeck, C. Wylock and P. Colinet, *Physics of Fluids*, 2009, **21**, 091108.
71. P. Giacomo, *Metrologia*, 1982, **18**, 33.
72. A. Picard, R. S. Davis, M. Gläser and K. Fujii, *Metrologia*, 2008, **45**, 149.
73. N. Shahidzadeh-Bonn, S. Rafaï, A. Z. A. Azouni and D. Bonn, *Journal of Fluid Mechanics*, 2006, **549**, 307-313.
74. P. L. Kelly-Zion, C. J. Pursell, S. Vaidya and J. Batra, *Colloids and Surfaces A: Physicochemical and Engineering Aspects*, 2011, **381**, 31-36.
75. K. Sefiane, Y. Fukatani, Y. Takata and J. Kim, *Langmuir*, 2013, **29**, 9750-9760.
76. H. Ghasemi and C. A. Ward, *Physical Review Letters*, 2010, **105**, 136102.
77. P. M. Chaikin and T. C. Lubensky, *Principles of Condensed Matter Physics*, Cambridge University Press2000.

TOC

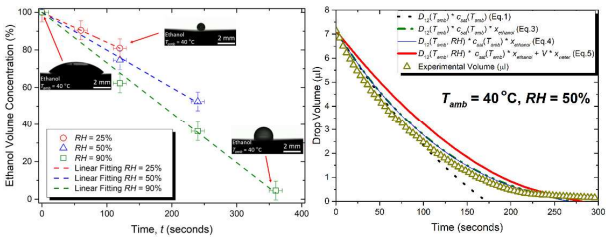

Simultaneous evaporation and water intake empirical model for evaporation of organic solvent ethanol drops